IEEE Access
Multidisciplinary | Rapid Review | Open Access Journal

Received 14 October 2023, accepted 30 October 2023, date of publication 2 November 2023,
date of current version 13 December 2023.

Digital Object Identifier 10.1109/ACCESS.2023.3329965

RESEARCH ARTICLE

CLLCLC Topology Based on Adaptive Excitation Inductance for the Improvement of Bidirectional DC–DC Converter Efficiency

LEI GUO[1], XIONGMING CHEN[1], JIAZHE CHEN[2], PENG LUO[1], (Member, IEEE), AND LIMING ZHAO[1]

[1]School of Electronic and Information Engineering, Guangdong Ocean University, Zhanjiang 524088, China
[2]Basic Experimental Teaching Centre, Guangdong University of Technology, Jieyang 522000, China

Corresponding authors: Jiazhe Chen (1636368187@163.com) and Peng Luo (dqluopeng@163.com)

This work was supported in part by the National Natural Science Foundation of China under Grant 62272109, and in part by the Program for Scientific Research Start-Up Funds of Guangdong Ocean University under Grant 060302112315 and Grant 060302112306.

ABSTRACT Due to the great uncertainty of the output power of renewable energy sources (RESs), the storage and reuse of RESs is the focus of new energy technology. The bidirectional DC-DC resonant converter is preferred in the new energy technology. However, the efficiency of traditional bidirectional DC-DC resonant converter will be greatly affected by the wide voltage gain range. By applying the adaptive excitation inductance, a CLLCLC resonant converter is proposed. The *L*-*C* branch is introduced to replace the fixed excitation inductance in traditional CLLLC resonant converter. In the design of transformer, the turns ratio and excitation inductance of transformer are decoupled to reduce the difficulty of transformer design. Simultaneously, compared with the traditional transformer, the impedance of equivalent excitation inductance will adjust automatically against the working frequency, decreasing the circulating current loss of resonant tank. Therefore, the proposed converter solves the contradiction between wide voltage gain range and high efficiency existed in the traditional converter. Finally, an experimental platform with 200 W rated power is built to verify the effectiveness of proposed topology.

INDEX TERMS Bidirectional dc–dc resonant converter, renewable energy sources (RESs), zero voltage switching (ZVS).

I. INTRODUCTION

Due to the energy crisis and environmental pollution, RESs such as solar energy, small wind turbine, and wave power generator are used [1], [2], [3], [4]. However, RESs have the characteristics of intermittent nature and unpredictability and output power changes dramatically under the influence of environmental factors. Therefore, the application of energy storage system can solve the problem of power supply imbalance in RESs to meet the requirements of normal operation.

Energy storage system is very important for the stable operation of RESs. And the charge and discharge of energy storage system efficiently and reliably have always been the focus of energy storage technology research. A bidirectional dc-dc converter with quadrants was proposed to realize two-way transmission of the energy because direction of input and output current can be changed when the polarity of input and output voltage is unchanged [5]. It is equivalent to two one-way DC converters in function. Compared with two single-phase DC/DC converters to achieve bidirectional energy transmission, bidirectional DC/DC converters have the advantages of high efficiency, small size, good dynamic performance and low cost. The volume weight and cost of the system can be greatly reduced, which attracts a lot of attention [6], [7], [8].

In the design of bidirectional DC/DC converters. the pulse frequency modulation (PFM) control is widely used in the DC/DC converter. The limitation of ordinary PFM control is

The associate editor coordinating the review of this manuscript and approving it for publication was Liu Hongchen.

that the operating frequency changes greatly with the increase of voltage gain range. In order to solve the problem of transmission efficiency degradation caused by a wide range of input voltages, a lot of researches have been carried out [9], [10], [11]. In fact, bidirectional converters also have other modulation strategies besides conventional pulse modulation (PFM), like phase shift modulation (PSM), pulse modulation (PWM), and resonant frequency modulation (RFM) [12], [13], [14]. By combining these different modulation strategies, hybrid modulation strategies can be proposed to narrow down the operating switching frequency range in range applications. In [15], the PSM+PFM modulation strategy is adopted for full-bridge LLC resonant converter in the Onboard Charger application (OBC); however, this hybrid modulation strategy requires additional resonant capacitors and switches. Moreover, the extension of the voltage gain range is insignificant, and these hybrid modulation strategies create difficulties in the analysis and design of LLC resonant converters.

The optimization on transformers is another important part to improve the transfer efficiency. The planar transformers (PT) capacitance issue is characterized in detail and mitigation strategies are proposed to improve the performance of LLC converters with PTs [16]. A novel matrix transformer structure is proposed to integrate four elemental transformers into one magnetic core with simple four-layer print circuit board windings implementation and further reduced core loss [17]. Efficient methods to design and optimize air-core planar transformers for high-frequency LLC converters are proposed to optimize the transfer efficiency [18]. Conclusions can be drawn from the similar paper [19], [20], [21]. In addition, a common problem in bidirectional resonant topology is that the controller often uses frequency modulation to regulate the output voltage. For a wide input application, a wide operational frequency range is usually required [6], [7], [8], [9], [10]. It is difficult to obtain an optimized design because the operational frequency is directly related to many types of converter losses [13], [14], [15]. Therefore, these converters are often used as solid-state transformers. Nevertheless, the excitation inductance of the solid-state transformers is fixed and not paid enough attention. In fact, the excitation inductance will participate in the resonant process of the resonant converter. And it will have a significant influence on the performance of DC/DC converter. According to the conventional design method, the high gain of LLC converter is often obtained at the expense of excitation inductance. However, smaller excitation inductor often leads to larger cavity current and lower efficiency [23]. Variable capacitors or inductors can be used to adjust the impendence of the resonant cavity [24], [25], [26], [27], [28], [29], [30]; however, the converters suffer from complex resonant cavities, high control difficulties, and many components, etc. A novel multi-resonant DC/DC converter with a notch filter is proposed in [24], which can use third harmonic to transmit the active power. The loss of the reactive power cycle is reduced, and efficiency is improved. However, the design of the parameters of the converter becomes complicated with the addition of resonant elements. In [25], a topology combines two LLC converters through coupled resonance to achieve wide-range operation, increasing the size and cost. Therefore, modification of the internal structure of the resonant cavity to obtain a wider input voltage range is worth investigating. The LLC converter with a variable resonant cavity for increased voltage gain range is proposed in [26]. However, the additional inductor and switch will make control more difficult and complex. In [27], by introducing LCLC resonant, the conventional LLC circuits improve voltage gain but did not analyze the effect of resonant elements on its high gain characteristics. In [28], [29], and [30], the efficiency of the converters is also improved, but the circuit structure is complex, and the control cost is high. In order to meet the requirements of wide gain and high efficiency, the CLLCLC topology based on adaptive excitation inductor is adopted in the bidirectional DC-DC converter. An L_p-C_p series network is used to replace the inherent excitation inductance of transformer. By properly designing the parameters L_p and C_p, the equivalent excitation inductance can always remain inductive when the switching frequency is greater than the minimum operating frequency f_{smin} (full range ZVS can be realized), and the equivalent excitation inductance can increase with the increasing of the operating frequency. Therefore, when the input voltage is low, the switching frequency is small and the equivalent excitation inductance is small, so the converter can provide higher gain; when the input voltage is high, the switching frequency is large and the equivalent excitation inductance is large, so the converter has a higher efficiency. The gain plot of CLLCLC is modified with a sharper shape than the conventional CLLLC converter. Under the same gain range, the narrow operational frequency range makes the design and optimization easier and more flexible. In addition, the contradiction between the wide voltage gain range and the high efficiency of the traditional converter can be solved by introducing only one capacitor, which greatly reduces the design cost of the converter as well as the control difficulty. Besides, the transformer in CLLCLC converter is an ideal transformer, which means the transformer design process doesn't need much effort. Consequently, the proposed converter has a simple circuit structure, low component count, low control difficulty, and a wide voltage gain range, making it applicable in the energy storage charge/discharge systems, such as batteries, ultracapacitors, electric vehicles (EV), microgrids, and uninterruptible power supplies.

The rest of the paper is organized as follows, the proposed topology and operating principles are presented in Section II. Then in Section III, the para meter design process, the impedance characteristic of equivalent excitation inductance and efficiency analysis are discussed. Section IV presents the experimental results and corresponding analyses of the results. Finally, the conclusion is given in Section V.

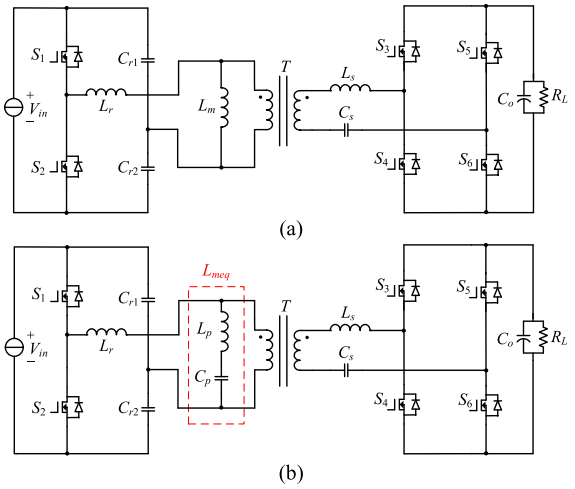

FIGURE 1. Topology of the bidirectional resonant dc–dc converter. (a) The conventional CLLLC resonant converter. (b) The proposed CLLCLC resonant converter based on the adaptive excitation inductor.

II. FUNDAMENTAL ANALYSIS

The proposed bidirectional CLLCLC resonant converter is based on the traditional CLLLC resonant converter, therefore, the working mode is similar with the operation state of traditional CLLLC resonant converter.

A. PROPOSED TOPOLOGY

The circuit structure of the bidirectional resonant dc–dc converter is shown in Fig.1. The conventional CLLLC resonant converter is shown in Fig.1(a). It consists of energy conversion modules in the primary side and secondary side, and the resonant network to connect them. The energy conversion modules can be used for inverter or rectifier according to the energy flow direction. The CLLLC resonant tank in the primary side is composed of the resonant inductor L_r, the separated resonant capacitors C_{r1} and C_{r2}, and the excitation inductors L_m comes from the transformer. The design of split resonant capacitor C_{r1} and C_{r2} can effectively reduce the current stress of a single capacitor C_r and improve the EMI characteristics of the converter. Compared with conventional CLLLC resonant converter, the biggest difference of proposed CLLCLC converter lies in the use of equivalent excitation inductance L_{meq}. An L_p-C_p series resonant branch replaces the excitation inductance L_m. Compared with the fixed excitation inductor in the traditional transformer, the impedance of the equivalent excitation inductor composed of L_p-C_p series branches increases with the increasing of the resonant frequency, which will reduce the excitation current and the circulating current loss of the resonant tank. Therefore, compared with the traditional CLLLC converter, the proposed converter solves the contradiction between wide voltage gain range and high efficiency in bidirectional CLLLC resonant converter, and improves the rated point efficiency of the converter.

For the bidirectional CLLCLC converter based on adaptive excitation inductor, according to the energy flow direction,

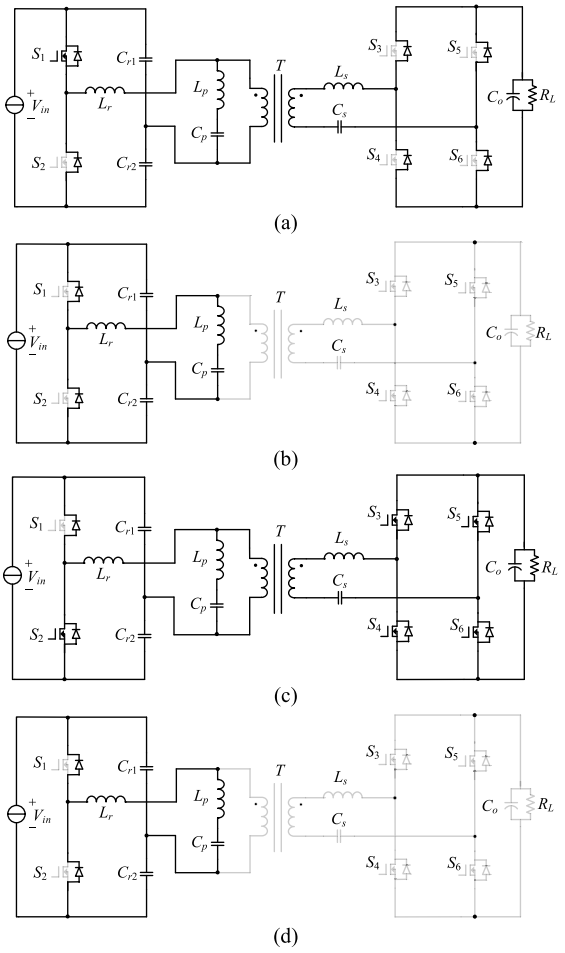

FIGURE 2. Equivalent circuits for each stage under Step-Up directions of the power flow. (a) Mode 1 (t_0-t_1). (b) Mode 2 (t_1-t_2). (c) Mode 3 (t_2-t_3). (d) Mode 4(t_3-t_4).

the control strategy of the primary and secondary side energy conversion module can be expressed as follows:

1) When the converter works in the step-up direction or backward mode, S_1 and S_2 constitute a half bridge circuit, which is responsible for converting the input DC voltage source into a square wave with frequency f_s and duty cycle of 50%. Normally, in order to prevent the upper and lower bridge arms from conducting at the same time, a small dead time is inserted between them. Simultaneously, the driving signals of the secondary switches S_3, S_4, S_5 and S_6 are not given, and their body diodes are only used for making up a full bridge rectification.
2) When the converter works in the step-down direction or forward mode, the pulse frequency modulation (PFM) control strategy is used for the secondary switches S_3, S_4, S_5 and S_6, while the primary switches S_1 and S_2 are turned off, and only their body diodes forms the voltage doubling rectification.

After the above topology improvement and corresponding control, the proposed bidirectional CLLCLC converter based

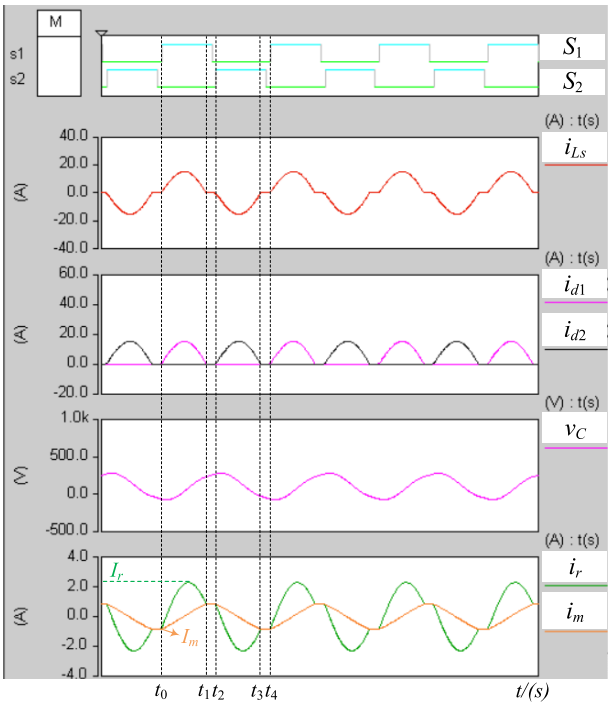

FIGURE 3. Operation principles of the proposed CLLCLC resonant tank with the step-up directions of the power flow.

on adaptive excitation inductor can achieve high efficiency energy conversion in a wide voltage gain range.

B. OPERATION PRINCIPLES

Some assumptions are set before the analysis process as follows.

1) The switches, inductors, capacitors and voltage source are ideal devices.

2) The primary and secondary leakage inductances of power transformer are ignored.

The operation principle of the proposed CLLCLC resonant converter is similar to the conventional LLC resonant converter.

1) FORWARD MODE

The Fig.2 and Fig.3 are the equivalent circuit of each mode and some significant waveforms in step-up mode, respectively.

a: MODE 1 (t_0-t_1)

When the S_1 is turned ON and S_2 is turned OFF, the body diodes of the secondary switches S_3, S_4, S_5 and S_6 work as a full bridge rectification. The energy is transferred to the secondary side via the transformer. The equivalent synchronous rectifier is on, and the output capacitance is large enough so that the output voltage can be seen as V_o. The ideal transformer converts the voltage V_{oL} of the secondary side to the primary side, therefore, the primary side voltage is nV_o, furthermore, the excitation current rises due to the choke of output capacitor. Simultaneously, the C_{r1}, C_{r2} and L_r are in resonant state.

The resonant current i_r, the excitation current i_m and the resonant capacitor voltage V_c can be expressed as:

$$\begin{cases} i_r(t) = I_r \sin(\omega t + \theta) \\ i_m(t) = I_m + \dfrac{nV_o}{L_m} \\ V_c(t) = -\omega L_r I_r \cos(\omega t + \theta) - nV_o + V_{in} \\ \omega = \dfrac{1}{\sqrt{L_r(C_{r1} + C_{r2})}} \end{cases} \tag{1}$$

b: MODE 2 (t_1 -t_2)

With the increasing of excitation current i_m, the resonant current will hit the excitation current i_m at t_1. Therefore, there is no energy transferred to the secondary side. And the equivalent inductor branch will not be choked by the output capacitor, as a result, the L_p and C_p will participate in the resonant state of L_r and C_r.

$$\begin{cases} i_r(t) = I_r \sin(\omega t + \theta) \\ i_m(t) = i_r(t) \\ V_c(t) = -\omega L_r I_r \cos(\omega t + \theta) + V_{in} \\ \omega_1 = \dfrac{1}{\sqrt{(L_r + L_m)(C_{r1} + C_{r2})}} \end{cases} \tag{2}$$

c: MODE 3 (t_2 -t_3)

When the S_1 is turned OFF and S_2 is turned ON, the body diodes of the secondary switches S_3, S_4, S_5 and S_6 work as a full bridge rectification. The energy is transferred to the secondary side via the transformer again. The output voltage can be seen as V_o due to the existence of filter capacitor. The ideal transformer converts the voltage -V_o of the secondary side to the primary side, therefore, the primary side voltage is -nV_o, furthermore, the excitation current decreases due to -nV_o. Simultaneously, the C_{r1}, C_{r2} and L_r are in resonant state. The resonant current i_r, the excitation current i_m and the resonant capacitor voltage V_c can be expressed as:

$$\begin{cases} i_r(t) = I_r \sin(\omega t + \theta) \\ i_m(t) = I_m + \dfrac{nV_o}{L_m}(t_1 - t_0 - t_3 + t_2) \\ V_c(t) = -\omega L_r I_r \cos(\omega t + \theta) - nV_o + V_{in} \\ \omega = \dfrac{1}{\sqrt{L_r(C_{r1} + C_{r2})}} \end{cases} \tag{3}$$

d: MODE 4 (t_3-t_4)

Then the resonant current i_r and the excitation current i_m will meet again in t_3. The excitation current keeps the same with the resonant current. Therefore, there is no energy transferred to the secondary side. And the equivalent excitation inductor branch will not be choked by the voltage of secondary side, then the L_p and C_p will participate in the resonant state of L_r

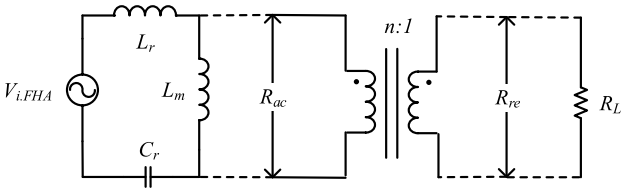

FIGURE 4. The equivalent circuit model after the FHA method.

and C_r, which is similar with mode 2.

$$\begin{cases} i_r(t) = I_r \sin(\omega t + \theta) \\ i_m(t) = i_r(t) \\ V_c(t) = -\omega L_r I_r \cos(\omega t + \theta) + V_{in} \\ \omega_1 = \dfrac{1}{\sqrt{(L_r + L_m)(C_{r1} + C_{r2})}} \end{cases} \tag{4}$$

According to the continuity of inductor current and capacitor voltage at the crossing point of four modes, the resonant current i_r and the excitation current i_m can be derived out.

Besides, the analysis process of step-down mode is similar with that of step-up mode. And it will not be described again.

III. DESIGN OF THE PROPOSED CLLCLC CONVERTER

A. PARAMETERS DESIGN

To design a wide input resonant converter, the gain frequency curve must be given first. The gain calculation methods of resonant converter mainly include extended function description method (EDF), fundamental wave equivalent method (FHA) and numerical calculation method (saber simulation or modal analysis). The LLC gain calculation process can be simplified by using FHA method. The disadvantage is that the accuracy decreases when operation frequency deviates far from the resonant frequency. The advantages of EDF and numerical calculation have a high accuracy, but the large amount of calculation increase the workload. The wide input resonant converter needs iteration repeatedly to obtain the gain curve, the calculation is heavier. Therefore, FHA method is used to calculate the single point gain, which shortens the iteration time.

The proposed equivalent circuit model after FHA method is shown in Fig.4. There are three resonant elements (C_r, L_m, L_r) and resistor R_{ac}. R_{ac} is the equivalent resistance in the primary side of the transformer.

The relationship between R_{ac} and R_L is shown in equation (5), where n is the turn ratio of the transformer.

$$R_{ac} = \frac{8n^2}{\pi^2} R_L \tag{5}$$

There are two resonant frequencies f_r and f_{r1} due to the existing of three resonant parameters. When the synchronous rectifier operates, the L_m does not participate in the resonance with C_r and L_r, then the resonance frequency is f_r. When the synchronous rectifier does not work, L_m and L_r are in resonant state with C_r, and then the resonance frequency is f_{r1}. The expressions of two operation frequencies are

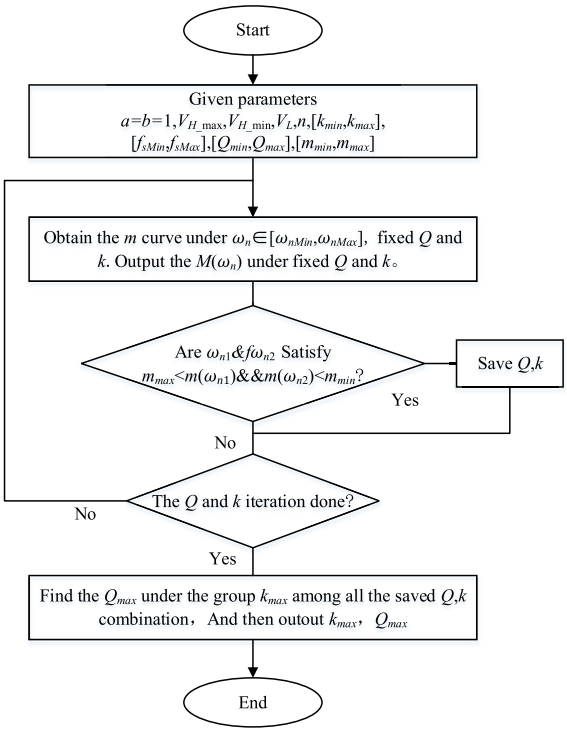

FIGURE 5. The flow chart of wide input design method for LLC resonant converter.

presented as

$$f_r = \frac{1}{2\pi\sqrt{L_r C_r}} \tag{6}$$

$$f_{r1} = \frac{1}{2\pi\sqrt{(L_r + L_m) C_r}} \tag{7}$$

The resonant tank characteristics of LLC can be evaluated according to the quality factor Q and the ratio k of inductance L_m to L_r. The larger the k value is, the larger the frequency interval between f_r and f_{r1} is. The definition of k value is shown in equation 8. The larger the Q value is, the smaller the resonant tank current is and the higher the efficiency is. The definition of Q value is shown in equation (9).

$$k = \frac{L_m}{L_r} \tag{8}$$

$$Q = \frac{\sqrt{L_r / C_r}}{R_{ac}} \tag{9}$$

The formula of gain m by the FHA method is given without deduction according to [22], and it is expressed as

$$m_{forword} = \frac{1}{n} \cdot \frac{1}{\sqrt{\alpha^2 + \beta^2}} \tag{10}$$

where

$$\alpha = \frac{1}{k} + \frac{1}{k\omega_n^2} + 1$$

$$\beta = \frac{1}{\omega_n}\left(\frac{\alpha}{k} + \frac{1}{kb} + \frac{1}{b} + 1\right)Q - \omega_n\left(\frac{\alpha}{k} + \alpha + 1\right) - \frac{Q}{kb} \cdot \frac{1}{\omega_n^3} \tag{11}$$

TABLE 1. Comparison of the proposed converter with [24], [25], [26], [27], [28], [29], and [30].

Topology	Modulation	Frequency Range	Voltage Range	System Gain M	Output Power	Peak Efficiency
LC-LC[24]	PFM	55 kHz~110 kHz	330 V~390 V	1~1.2	2500 W	95 %
LLC-LLC[25]	PFM	200 kHz~400 kHz	260 V~340 V	1.3~1.7	240 W	94.3 %
LLC[26]	on/off	50 kHz~400 kHz	290 V~405 V	1.5~2.0	350 W	95 %
LCLC[27]	PFM	135 kHz~250 kHz	250 V~400 V	1.2~2.0	500 W	96.4 %
LLC-LLC[28]	PFM	88 kHz~133 kHz	45 V~135 V	0.7~2.0	230 W	95.5 %
CL-LLC[29]	PFM	400 kHz~600 kHz	350 V~500 V	0.9~1.3	400 W	95.9 %
LLC-LLC[30]	PFM	85 kHz~165 kHz	50 V~300 V	0.4~2.3	250 W	95 %
Proposed	PFM	320 kHz~500 kHz	250 V~350 V	1.5~2.1	200 W	97.8 %

f_n and ω_n are the normalized switching frequency and normalized angular frequency, $f_n = f_s/f_r$, $\omega_n = 2\pi f_n$.

It can be seen from (10) that the gain m is related to the value of k, the turn ratio of transformer n, the quality factor Q, the ratio of L_r, n^2L_s, a, the ratio of C_s, n^2C_r b, and the turn ratio n is determined, $a = b = 1$, the corresponding gain m can be obtained by inputting ω_n, Q and k, On the contrary, when the maximum gain range $[m_{\min}, m_{\max}]$ and the normalized angular frequency range $[\omega_{\min}, \omega_{\max}]$ are determined, the Q, k value combination satisfying the above conditions can be obtained by iterating (10). For the wide input resonant converter, the gain range $[m_{\min}, m_{\max}]$ should be satisfied firstly, then taking the efficiency into consideration (find the largest k value k_{max} among all the Q, k value combinations that meet the conditions) should be taken into account. The flow chart of wide input resonant converter design method is shown in Fig.5. Furthermore, the parameters of the resonant networks are obtained by the relationship between k, Q and C_r, L_m, L_r and R_{ac}. And they are shown as.

$$\begin{aligned} C_r &= 1/2\pi f_s R_{ac} Q \\ L_r &= R_{ac}^2 Q^2 C \\ L_m &= kL_r \end{aligned} \tag{12}$$

B. PARAMETERS CONVERSION OF L_m TO L_p-C_p

In the traditional CLLLC resonant converter, the excitation inductor L_m is fixed. Then with the decreasing of the operation frequency, the equivalent impedance of the whole resonant tank will increase, which will lead a higher excitation current and increase the power loss. By comparison, the replacement of L_m by a L_p-C_p branch has a flexible impedance against the operation frequency. When CLLLC resonant tank is converted to CLLCLC, C_p and equivalent excitation inductance L_{meq} at minimum operating frequency should be paid more attention. From (13), it can be seen that when C_p is small, L_{meq} is higher, the excitation current is smaller and a higher efficiency can be obtained. Besides, to ensure the maximum gain requirement, L_{meq} (f_{smin}) should be equal to the fixed excitation inductance L_m in CLLLC resonant tank, as shown in (14).

$$L_{meq}(f_s) = L_p - \frac{1}{(2\pi f_s)^2 C_p} \tag{13}$$

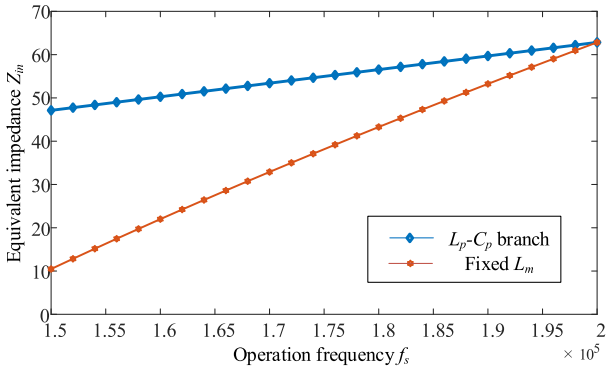

FIGURE 6. The equivalent impedance in LCLC and LLC resonant tank.

$$L_{meq}(f_{s\min}) = L_p - \frac{1}{(2\pi f_{s\min})^2 C_p} = L_m \tag{14}$$

However, the value of C_p should not be too small. A smaller value C_p will bring a larger voltage stress across the capacitance C_p. As shown in (15), V_{Cp_pk} is the peak-to-peak voltage of capacitance C_p, and the maximum value appears when $f_s = f_{smin}$. Considering the voltage stress on C_p and the effect of C_p on improve the transmission efficiency, the value of C_p needs to be chosen properly.

$$V_{Cp\_pk} = \frac{4nV_o}{\pi} \cdot \frac{1}{(2\pi f_{s\min})^2 L_p C_p - 1} \tag{15}$$

For the consideration of device selection, C_p and C_r can be selected according to the same withstand voltage. gives the peak-to-peak voltage V_{Cr} of C_r is given as follows.

$$V_{Cr\_pk} = \frac{P_{out}}{2C_r V_{in\_\min} f_{s\min}} \tag{16}$$

L_p and C_p can be obtained by considering the (14), (15) and (16), which is the conversion from L_m parameters to L_{meq} parameters.

The equivalent impedance in CLLLC and CLLCLC resonant tank are shown in Fig.6. Obviously, the equivalent impedance of CLLCLC resonant tank changes slowly with the decreasing of operation frequency, which means a smaller excitation current and higher transmission efficiency during the whole operation process.

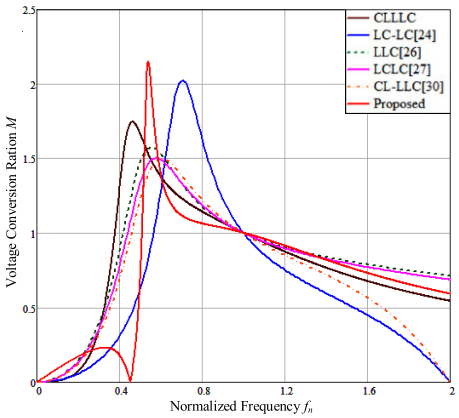

FIGURE 7. The voltage conversion ratio versus normalized frequency of the proposed converter and relevant converters under P_o =200 W.

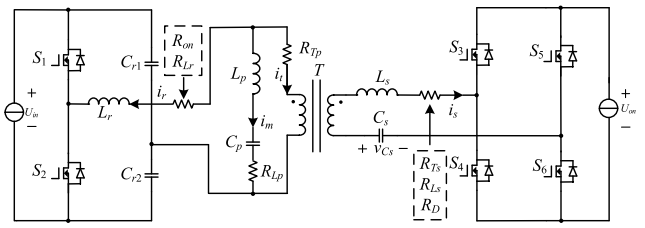

FIGURE 8. Simplified loss model of LCLC converter.

In Table 1, the comparison with the proposed converter and the converters in [24], [26], [27], and [30], including modulation strategy, frequency range, voltage range, system gain, output power, and peak efficiency, it can be seen that the proposed topology has a significant advantage in efficiency and can satisfy a wide gain while maintaining high efficiency. In addition, the voltage gain comparison with other latest existing converters under $P_o = 200$ W in Fig.7, the proposed converter has a higher gain and a narrower operating frequency range under the same input voltage and load current, making the design and optimization of the converter easier and more flexible.

C. POWER LOSS MODEL OF PROPOSED CONVERTER

Loss estimation is important for heat dissipation design and efficiency optimization in converter design. By establishing the loss model of the proposed converter and combining the loss model with the modal solver, the losses of the converter can be calculated,

A simplified model for calculating the losses of CLLCLC converters is shown in Fig.8.

The power loss of the converter includes conduction loss, switching loss, ferrite loss, and other losses [31]. The other loss is mainly caused by the driving circuit and the equivalent series resistors (ESRs) of the printed circuit board (PCB).

The conduction loss $P_{c,loss}$ can be expresses as

$$P_{c,loss} = I_r^2(R_{Lr} + R_{on}) + I_m^2 R_{Lp} + I_t^2 R_{Tp} + I_s^2(R_{Ls} + R_{Ts}) + V_{F,d} I_{d,avg} \quad (17)$$

TABLE 2. Specification of prototype.

Circuit parameters	Value
High voltage side (V_H)	250-350 V
Low voltage side (V_L)	24 V
Rated high voltage side current (I_H)	0.7 A
Rated low voltage side current (I_L)	8.3 A
Rated output power (P_o)	200 W
Switching frequency (f_s)	320~500 kHz

where I_r, I_m, I_t, and I_s are RMS resonant current, excitation current, transformer primary windings' current, and transformer secondary windings' current, respectively. $I_{d,avg}$ is diode's average current. R_{Lr}, R_{Lp}, R_{Ls}, R_{Tp}, R_{Ts} are the ESRs of resonant inductor, primary excitation inductor, secondary excitation inductor, primary and the secondary windings, respectively. R_{on} is the on-resistor of MOSFETs. $V_{F,d}$ is the forward voltage-drop of diodes.

The switching loss $P_{s,loss}$ can be expresses as

$$P_{S,loss} = 0.5 \times I_{s,off} U_{in} t_{fall} f_s + I_s^2 R_D \quad (18)$$

where $I_{s,off}$ and t_{fall} are the turn-off current and fall-time of MOSFETs, respectively. $I_{s,off} = i_r(0.5T_s)$, R_D is the on-resistor of diode. Based on [32], The ferrite loss $P_{fe,loss}$ is obtained as

$$P_{fe,loss} = V_T K_T \Delta B_T^{\alpha T} f_S^{\beta T} + V_{Lr} K_{Lr} \Delta B_T^{\alpha T} f_S^{\beta T} + V_{Lp} K_{Lp} \Delta B_T^{\alpha T} f_S^{\beta T} + V_{Ls} K_{Ls} \Delta B_T^{\alpha T} f_S^{\beta T} \quad (19)$$

where V_T, V_{Lr}, V_{Lp} and V_{Ls} are the cores' volume of transformers and inductors, respectively. K_T, α_T and β_T are parameters representing the property of transformers' cores. K_{Lr}, V_{Lp}, V_{Ls}, α_{Lr} and β_{Lr} are parameters representing the property of resonant inductors' cores. ΔB_T and ΔB_{Lr} are the flux density swings of transformers and resonant inductors, $\Delta B = 2\mu_0\mu_e N_{turn} I_{max}/l_e$. μ_0 and μ_e are the space and effective permeabilities, respectively. N_{turn} is turn number. I_{max} is the maximum current of windings. l_e is the effective magnetic loop length.

The other loss $P_{ot,loss}$ mainly consists of the driving loss and the PCB ESR's loss. $P_{ot,loss}$ is derived as

$$P_{ot,loss} = P_{dr,loss} + P_{esr,loss} = 2Q_g U_{dr} f_s + I_{esr}^2 R_{esr} \quad (20)$$

where $P_{dr,loss}$ and $P_{esr,loss}$ are the driving loss and the PCB ESR's loss. Q_g is the MOSFET's charge. U_{dr} is the driving voltage. R_{esr} is the PCB's ESR. I_{esr} is the current flowing through R_{esr}. The theoretical efficiency η can be concluded as

$$\eta = \frac{P_o}{P_o + P_{c,loss} + P_{s,loss} + P_{fe,loss} + P_{ot,loss}} \times 100\% \quad (21)$$

IV. EXPEROMENTAL RESULTS

A 200 W prototype, which can be employed for bidirectional applications with 250 V - 350 V high voltage port to 24 V

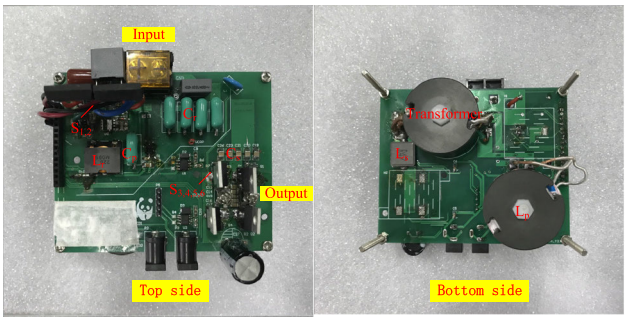

FIGURE 9. The image of prototype.

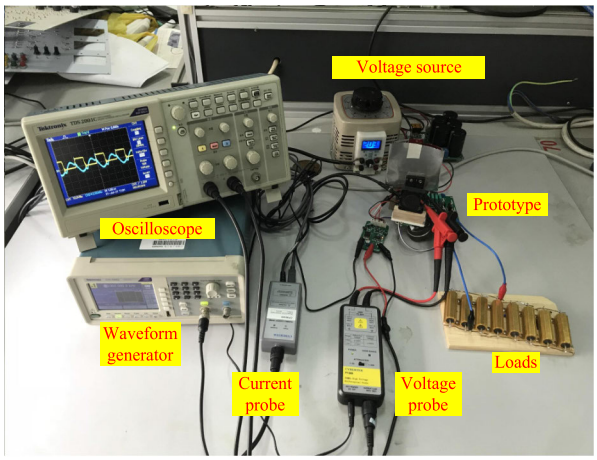

FIGURE 10. The Experimental setup of the prototype.

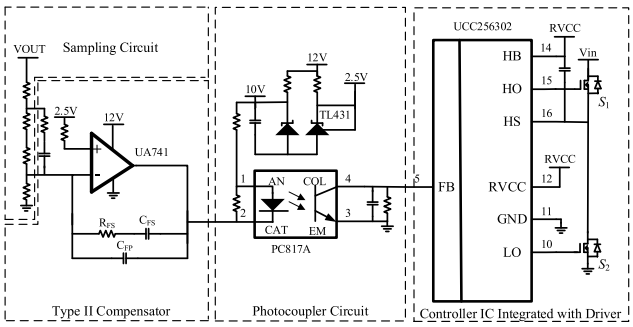

FIGURE 11. The control circuit of the proposed converter.

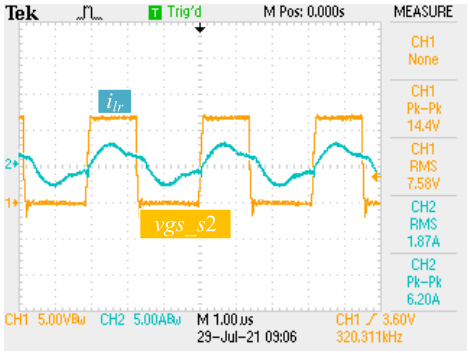

(a)

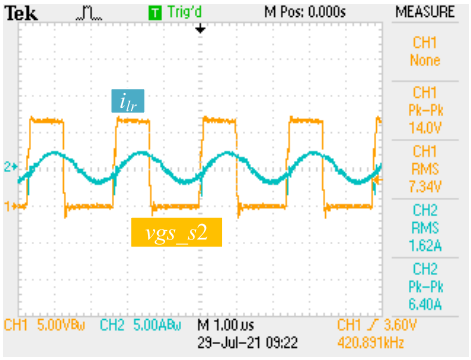

(b)

FIGURE 12. Experimental waveforms of CLLCLC converter in forward mode under full load, (a) V_H =400V (b) V_H =300V.

low voltage port is designed to verify its operation principle and advantage of introducing LC branch. The specification of prototype is shown in Table 2. The image of prototype is shown in Fig.9, and the experimental setup of the proposed converter system is shown in Fig 10.

The control method employed for the proposed converter is pulse frequency modulation (PFM). To realize the system's high efficiency and good dynamics, the control structure comprises four parts, as depicted in Fig.11., the sampling circuit, the Type II compensator, the photocoupler circuit, and the controller IC integrated with the driver. The controller works in four main processes. First, the output voltage is sampled through a divided voltage resistive. Second, the sampled voltage signal is passed through a Type II compensator. This compensator provides 0° to 90° phase boost with zero steady-state error. With proper tuning of this compensator, the converter performs a faster response, with minimal overshoots and zero steady-state error. To meet system requirements, the Type II compensator consisting of op-amp UA741, resistor R_{FS}, and capacitors C_{FS} and C_{FP} with values of 300 Ω, 0.1 uF, and 3.3 nF, respectively. Third, photocoupler chip PC817 is chosen to isolate the sampled signal. Fourth, the signal goes to IC UCC256302, a pulse frequency modulation (PFM) square wave with an approximately 50% duty cycle generated, which can be used for driving the switches.

The resonant frequency f_s is set to 500 kHz to guarantee the operation region of prototype located on $f_r < f_s$ and both ZVS of primary switches and ZCS of secondary switches are achieved. In order to fulfill the gain requirements, the values of k, Q set to $k = 3$, $Q = 0.4$. According to the above equation and from personal design experience. The primary resonant capacitor and resonant inductor have been selected as $C_{r1} = C_{r2} = 2.4$ nF, and $L_r = 22$ µH. The secondary resonant parameters have been calculated as $C_s = 227$ nF, $L_s = 449$ nH, finally, it is selected as $C_s = 235$ nF (47 nF*5), $L_s = 470$ nH. From $k = 3$, the L_m is designed to 66 µH. Using L_p-C_p to replace L_m to make sure L_{meq} (f_{smin}) equals L_m based on the FHA model, the current in the L_p-C_p branch can be calculated by (22) where I_{Cp_pk} is the peak value of the

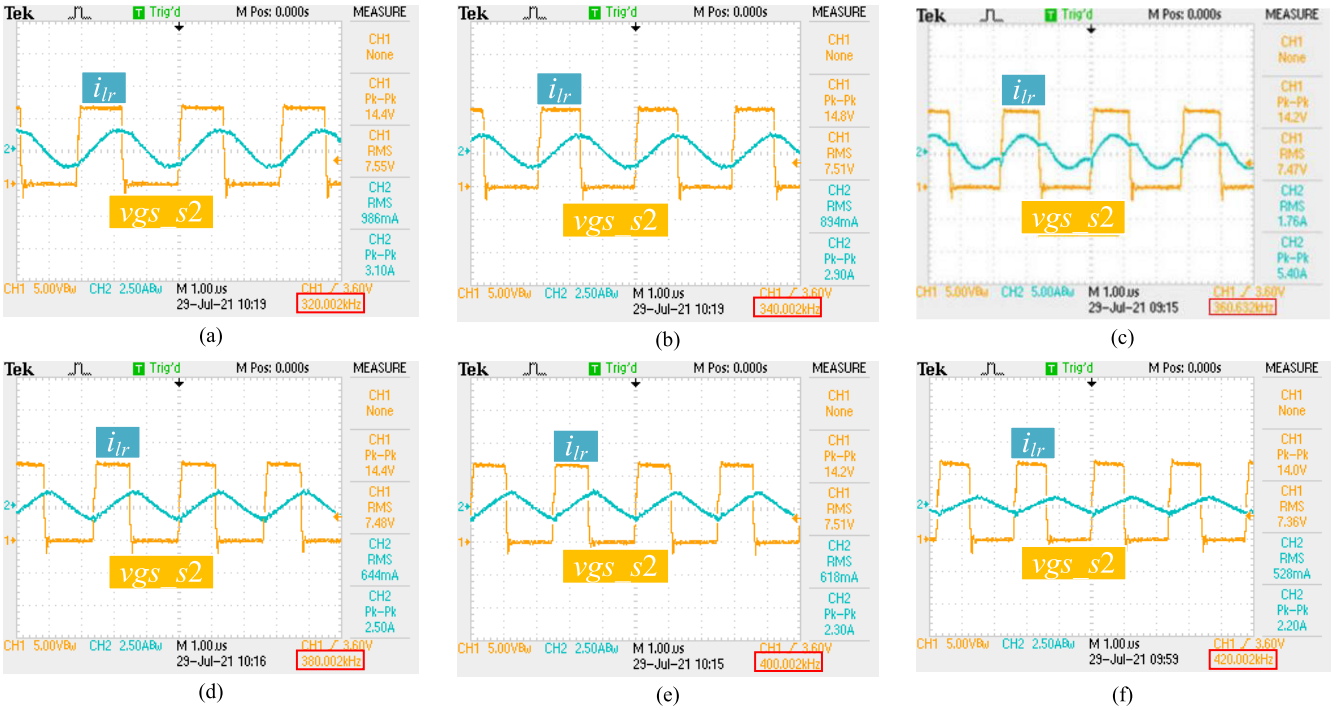

FIGURE 13. The waves of i_{Lmeq} at different operational frequency f_s.

TABLE 3. Parameters and components of the prototype.

Parameters	Values	Part numbers
resonant capacitor C_r	4.8 nF	4*1.2 nF CBB
resonant capacitor C_s	235 nF	5*47 nF MLCC
Resonant inductor L_r	22 μH	220MC-125
Resonant inductor L_s	470 nH	IHLP5050CEERR47M01
Branch inductor L_p	150 μH	custom made with GU36 core
Branch capacitor C_p	3.3 nF	1*3.3 nF CBB
Transformer T's n_p/n_s	21:3	Custom made with GU36 core
Primary switches	$S1$-$S2$	C2M0080120D
Secondary switches	$S3$-$S6$	IRFB3607

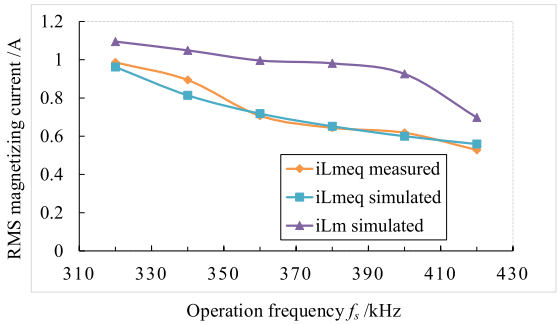

FIGURE 14. The RMS current i_{Lmeq} and i_{Lm} at operational frequency f_s.

L_p-C_p branch at f_{smin}.

$$I_{Cp\_\mathrm{pk}} = \frac{4}{\pi} nV_o \cdot \frac{1}{2\pi f_{s\,\min} L_m} \tag{22}$$

The AC peak voltage stress for a given C_p value can be calculated by (23), where V_{Cp_pk} is the peak value of the C_p voltage stress at f_{smin}.

$$V_{Cp\_\mathrm{pk}} = I_{Cp\_\mathrm{pk}} X_{Cp} = \frac{I_{Cp\_\mathrm{pk}}}{2\pi f_{s\,\min} C_p} \tag{23}$$

Substitute in (24) with $n = 7$, V_o of 24V, f_{smin} of 320 kHz, and 66 μH as L_m, and 250 V as peak voltage stress, the C_p value is 3.3 nF.

$$C_p = \frac{nV_o}{\pi^3 f_{s\,\min}^2 L_m V_{Cp\_\mathrm{pk}}} \approx 3.3\mathrm{nF} \tag{24}$$

For a given C_p, there is one and only one L_p that pairs with it. The L_p value can be calculated by (14) with 66 μH as L_m, 320 kHz as f_{smin}, and 3.3 nF as C_p, in this example, L_p is 150 μH.

To design L_p, the inductor turns is the most critical. It can be calculated from (25), with 150 μH as L_{max}, $I_{Lpeak} = I_{Cp\_pk} = 2$ A, 380 mT as B, and 207 mm^2 as A_e, where B is the saturation flux density of the high-power ferrite PC40 at 100 °C, and A_e is the effective cross-sectional area with GU36 core.

$$N = \frac{L_{\max} \cdot I_{Lpeak}}{0.7B \cdot \eta \cdot A_e} = 16.86 \tag{25}$$

Parameters and components of the prototype converter is showed in Table 3.

Fig12. illustrates the CLLCLC circuit experimental waveforms in charging mode at different input voltage V_H. The

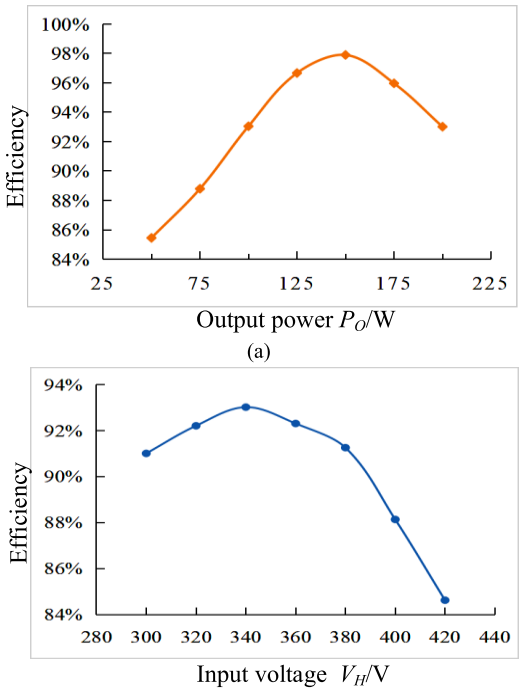

FIGURE 15. Measured efficiency at forward mode. (a) fixed V_H at different loads. (b) full load at different V_H.

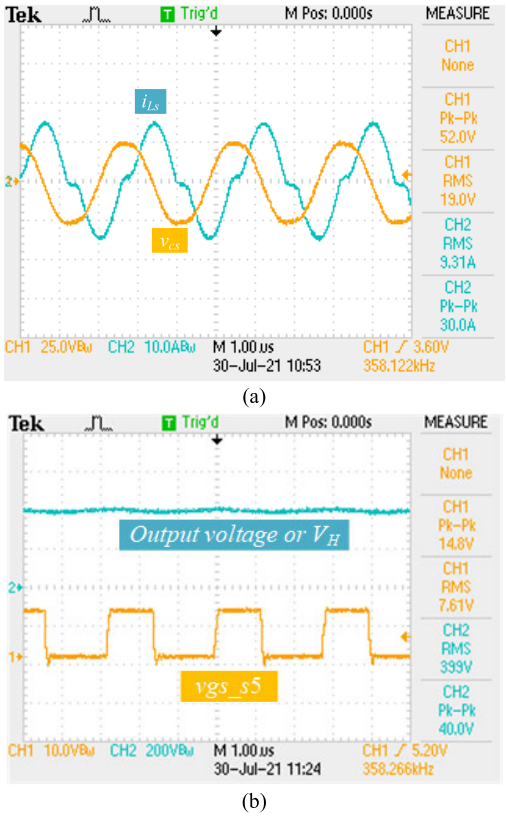

FIGURE 16. Waveforms at reverse mode. (a) C_S voltages and L_S current, (b) gate voltage of s_5 and output voltage.

output power is 200 W and $V_L = 24$ V. From the Fig.13, the current of L_r and the driving signal of S_2 is given, it is clear that, for all input voltage, i_{Lr} is negative when the S_2 is turned on, which ensures that the ZVS of S_1, S_2 is achieved. It is noted that the voltage of all switches will raise slowly from zero due to the existing of parallel output capacitor C_{oss}. Therefore, the quasi-ZVS turn-off is also realized. Besides, the operation frequency is adjusting automatically with the change of input voltage. The operation frequencies are 320.3 kHz and 420.9 kHz when the input voltage V_H are 400 V and 300 V, respectively.

Fig.14 illustrates the current waves of L_p, C_p branch i_{Lmeq} at different frequencies, the RMS value of i_{Lmeq} could be read from oscilloscope. From Fig13. the resonant current has almost no change with the frequency control method is proposed. To show the advantage of CLLCLC network more clearly, Fig14. comparing the RMS current values of fixed L_m (i_{Lm}) and L_p, C_p branch (i_{Lmeq}). Both i_{Lm} and i_{Lmeq} go down with the increasing of operational frequency, however, the fixed L_m one moves slowly than proposed one. Therefore, circulating current loss caused by resonant current, which have positive relationship with magnetizing current is reduced by introducing the L_p, C_p structure. It is noting that the improvement will be significant in the high-power applications.

Fig.15(a) shows the efficiencies of the built prototype under different load ranges, The maximum efficiency reaches up to 97.8% at 60% loads. Fig.15(b) shows the efficiencies of the prototype at different input voltage and the peak efficiency is 93.2% at $V_H = 340$V. The waveforms when the prototype operate in reverse mode under 24V input, 300V output, full load is showed in Fig.16. It is obvious that the step-up mode also works well for the proposed CLLCLC converter. Simultaneously, due to the completely symmetric topology structure, the ZVS of all active rectifier devices in reverse mode are realized too. In addition, the resonant tank current in the secondary side at step-down mode will also be reduced by the application of adaptive excitation inductor.

From the experimental results, the highest efficiency of the half-bridge CLLCLC converter is 97.8% in forward mode and 94% in reverse mode. The highest efficiency is achieved when prototype operates closed to f_r since the circulating loss is lowest at high frequency. Because the MOSFET body diode is used as a rectifier, the forward voltage of diode limits the peak efficiency. To optimize efficiency, synchronous rectifier is recommended in the design process.

V. CONCLUSION

This paper proposes a bidirectional CLLCLC DC-DC converter based on the adaptive excitation inductor for RESs. The content is mainly focused as follows:

(1) The operation principle of the proposed CLLCLC DC-DC converter is analyzed to verify the feasibility of forward and reverse modes. Simultaneously, the ZVS of all power devices is achieved.

(2) A L_p-C_p branch is introduced to replace the fixed excitation inductance in a traditional CLLLC resonant converter. As a result, the impedance of equivalent excitation inductance will adjust automatically against the working frequency,

which can reduce the circulating current loss of the resonant tank and further improve efficiency.

(3) The inherent excitation inductance of the transformer will not participate in the resonant process; therefore, the turns ratio and excitation inductance of the transformer are decoupled, greatly simplifying the design process of the transformer.

Finally, an experimental prototype of 200 W is implemented. The experimental results in the paper show that the maximum transmission efficiency can reach up to 97.8 % in the forward mode and 94 % in the reverse mode.

REFERENCES

[1] X. Sun, Y. Shen, Y. Zhu, and X. Guo, "Interleaved boost-integrated LLC resonant converter with fixed-frequency PWM control for renewable energy generation applications," *IEEE Trans. Power Electron.*, vol. 30, no. 8, pp. 4312–4326, Aug. 2015.

[2] S.-M. Chen, T.-J. Liang, and K.-R. Hu, "Design, analysis, and implementation of solar power optimizer for DC distribution system," *IEEE Trans. Power Electron.*, vol. 28, no. 4, pp. 1764–1772, Apr. 2013.

[3] Y. Xuan, X. Yang, W. Chen, T. Liu, and X. Hao, "A novel three-level CLLC resonant DC–DC converter for bidirectional EV charger in DC microgrids," *IEEE Trans. Ind. Electron.*, vol. 68, no. 3, pp. 2334–2344, Mar. 2021.

[4] P. K. Joseph and E. Devaraj, "Design of hybrid forward boost converter for renewable energy powered electric vehicle charging applications," *IET Power Electron.*, vol. 12, no. 8, pp. 2015–2021, Jun. 2019.

[5] V. F. Pires, D. Foito, and A. Cordeiro, "A DC–DC converter with quadratic gain and bidirectional capability for batteries/supercapacitors," *IEEE Trans. Ind. Appl.*, vol. 54, no. 1, pp. 274–285, Jan. 2018.

[6] Y.-E. Wu and Y.-T. Ke, "A novel bidirectional isolated DC–DC converter with high voltage gain and wide input voltage," *IEEE Trans. Power Electron.*, vol. 36, no. 7, pp. 7973–7985, Jul. 2021.

[7] Y. Shen, H. Wang, A. Al-Durra, Z. Qin, and F. Blaabjerg, "A bidirectional resonant DC–DC converter suitable for wide voltage gain range," *IEEE Trans. Power Electron.*, vol. 33, no. 4, pp. 2957–2975, Apr. 2018.

[8] J. Liu, "Impedance analysis of battery bidirectional DC–DC converter," *IEEE Access*, vol. 8, pp. 30960–30968, 2020.

[9] X. Ma, P. Wang, H. Bi, and Z. Wang, "A bidirectional LLCL resonant DC–DC converter with reduced resonant tank currents and reduced voltage stress of the resonant capacitor," *IEEE Access*, vol. 8, pp. 125549–125564, 2020.

[10] S. Zong, G. Fan, and X. Yang, "Double voltage rectification modulation for bidirectional DC/DC resonant converters for wide voltage range operation," *IEEE Trans. Power Electron.*, vol. 34, no. 7, pp. 6510–6521, Jul. 2019.

[11] Y.-F. Wang, B. Chen, Y. Hou, Z. Meng, and Y. Yang, "Analysis and design of a 1-MHz bidirectional multi-CLLC resonant DC–DC converter with GaN devices," *IEEE Trans. Ind. Electron.*, vol. 67, no. 2, pp. 1425–1434, Feb. 2020.

[12] K. Murata and F. Kurokawa, "An interleaved PFM LLC resonant converter with phase-shift compensation," *IEEE Trans. Power Electron.*, vol. 31, no. 3, pp. 2264–2272, Mar. 2016.

[13] J. Xu, J. Yang, G. Xu, T. Jiang, M. Su, Y. Sun, H. Wang, and M. Zheng, "PWM modulation and control strategy for LLC-DCX converter to achieve bidirectional power flow in facing with resonant parameters variation," *IEEE Access*, vol. 7, pp. 54693–54704, 2019.

[14] Y. Wei, Q. Luo, X. Du, N. Altin, A. Nasiri, and J. M. Alonso, "A dual half-bridge LLC resonant converter with magnetic control for battery charger application," *IEEE Trans. Power Electron.*, vol. 35, no. 2, pp. 2196–2207, Feb. 2020.

[15] S. Liu and F. Zhang, "State variable derivation with numerical approach and efficiency optimisation method for phase-shift LLC converters under wide voltage-gain range," *IET Power Electron.*, vol. 12, no. 7, pp. 1752–1762, Jun. 2019.

[16] M. A. Saket, N. Shafiei, and M. Ordonez, "LLC converters with planar transformers: Issues and mitigation," *IEEE Trans. Power Electron.*, vol. 32, no. 6, pp. 4524–4542, Jun. 2017.

[17] C. Fei, F. C. Lee, and Q. Li, "High-efficiency high-power-density LLC converter with an integrated planar matrix transformer for high-output current applications," *IEEE Trans. Ind. Electron.*, vol. 64, no. 11, pp. 9072–9082, Nov. 2017.

[18] G. K. Y. Ho, Y. Fang, and B. M. H. Pong, "A multiphysics design and optimization method for air-core planar transformers in high-frequency LLC resonant converters," *IEEE Trans. Ind. Electron.*, vol. 67, no. 2, pp. 1605–1614, Feb. 2020.

[19] M. Noah, S. Kimura, J. Imaoka, W. Martinez, S. Endo, M. Yamamoto, and K. Umetani, "Magnetic design and experimental evaluation of a commercially available single integrated transformer in three-phase LLC resonant converter," *IEEE Trans. Ind. Appl.*, vol. 54, no. 6, pp. 6190–6204, Nov. 2018.

[20] Z. Ouyang, Z. Zhang, M. A. E. Andersen, and O. C. Thomsen, "Four quadrants integrated transformers for dual-input isolated DC–DC converters," *IEEE Trans. Power Electron.*, vol. 27, no. 6, pp. 2697–2702, Jun. 2012.

[21] G. K. Y. Ho and B. M. H. Pong, "Multilayer flexible printed circuitry planar transformer with integrated series capacitance for an LLC converter," *IEEE Trans. Power Electron.*, vol. 34, no. 11, pp. 11139–11152, Nov. 2019.

[22] S. De Simone, C. Adragna, C. Spini, and G. Gattavari, "Design-oriented steady-state analysis of LLC resonant converters based on FHA," in *Proc. Int. Symp. Power Electron., Electr. Drives, Autom. Motion (SPEEDAM)*, May 2006, pp. 200–207.

[23] C.-S. Wang, S.-h. Zhang, Y.-f. Wang, B. Chen, and J.-h. Liu, "A 5-kW isolated high voltage conversion ratio bidirectional CLTC resonant DC–DC converter with wide gain range and high efficiency," *IEEE Trans. Power Electron.*, vol. 34, no. 1, pp. 340–355, Jan. 2019.

[24] Q. Zhao, W. Liu, Y. Wang, D. Wang, and N. Wu, "A novel multiresonant DC–DC converter with wide output-voltage range," *IEEE Trans. Power Electron.*, vol. 35, no. 6, pp. 5625–5638, Jun. 2020.

[25] T. Qian and C. Qian, "A combined topology with coupled LLC resonance for wide-range operation," *IEEE Trans. Power Electron.*, vol. 34, no. 7, pp. 6593–6600, Jul. 2019.

[26] Y. Jeong, M.-S. Lee, J.-D. Park, J.-K. Kim, and Ronald. A. L. Rorrer, "Hold-up time compensation circuit of half-bridge LLC resonant converter for high light-load efficiency," *IEEE Trans. Power Electron.*, vol. 35, no. 12, pp. 13126–13135, Dec. 2020.

[27] Y. Chen, H. Wang, Z. Hu, Y.-F. Liu, X. Liu, J. Afsharian, and Z. Yang, "LCLC converter with optimal capacitor utilization for hold-up mode operation," *IEEE Trans. Power Electron.*, vol. 34, no. 3, pp. 2385–2396, Mar. 2019.

[28] Y. Wei, Q. Luo, and H. A. Mantooth, "A novel LLC converter with topology morphing control for wide input voltage range application," *IEEE J. Emerg. Sel. Topics Power Electron.*, vol. 10, no. 2, pp. 1563–1574, Apr. 2022.

[29] X. Zhang, J. Jing, Y. Guan, M. Dai, Y. Wang, and D. Xu, "High-efficiency high-order CL-LLC DC/DC converter with wide input voltage range," *IEEE Trans. Power Electron.*, vol. 36, no. 9, pp. 10383–10394, Sep. 2021.

[30] Y. Wei, Q. Luo, and H. A. Mantooth, "An LLC converter with multiple operation modes for wide voltage gain range application," *IEEE Trans. Ind. Electron.*, vol. 68, no. 11, pp. 11111–11124, Nov. 2021.

[31] H. Xu, D. Chen, F. Xue, and X. Li, "Optimal design method of interleaved boost PFC for improving efficiency from switching frequency, boost inductor, and output voltage," *IEEE Trans. Power Electron.*, vol. 34, no. 7, pp. 6088–6107, Jul. 2019.

[32] S. M. S. I. Shakib and S. Mekhilef, "A frequency adaptive phase shift modulation control based LLC series resonant converter for wide input voltage applications," *IEEE Trans. Power Electron.*, vol. 32, no. 11, pp. 8360–8370, Nov. 2017.

LEI GUO received the Ph.D. degree in measuring and testing technologies and instruments from the Harbin University of Science and Technology, Harbin, China, in 2015.

Since 2015, he has been a Lecturer with the School of Electronics and Information Engineering, Guangdong Ocean University, Zhanjiang, China. His research interests mainly include the study on machine vision and power electronics.

XIONGMING CHEN was born in Guangdong, China, in 2002. He is currently pursuing the B.S. degree with Guangdong Ocean University, Zhanjiang, China. His current research interests include power electronics and renewable energy systems.

JIAZHE CHEN received the B.E. degree from the College of Physics and Information Engineering, Fuzhou University, Fuzhou, China, in 2016, and the M.E. degree from the School of Aerospace Engineering, Xiamen University, Xiamen, China, in 2020.

In September 2020, he joined as an Assistant Researcher with the Guangdong University of Technology. His research interests focus on the topology and control of resonant converters.

PENG LUO (Member, IEEE) received the M.S. degree in electrical engineering from the China University of Mining and Technology, Xuzhou, China, in 2015, and the Ph.D. degree in electrical engineering from the National Cheng Kung University, Taiwan, in 2023.

Since 2016, he has been with Guangdong Ocean University, China, where he has been a Lecturer, since 2019. From 2015 to 2016, he was an Assistant Electrical Engineer with China Nuclear Power Simulation Technology Corporation Ltd., Shenzhen, China. His research interests include power electronics converters and energy conversion.

LIMING ZHAO was born in Guizhou, China, in 1973. He received the M.S. degree in control theory and control engineering from the Anshan Institute of Steel and Iron Technology, Anshan, China, in 2004.

He is an Associate Professor with Guangdong Ocean University, China. His research interests include multi-source information fusion and intelligent control theory and application.